

**Investigation of the molecular causes underlying physical abnormalities in  
Diamond-Blackfan anemia patients with *RPL5* haploinsufficiency**

**Yuko Fukui<sup>1</sup>, Satoru Hayano<sup>1,2</sup>, Noriaki Kawanabe<sup>1</sup>, Ziyi Wang<sup>1,3</sup>, Akira  
Shimada<sup>4</sup>, Megumu K. Saito<sup>5</sup>, Isao Asaka<sup>6</sup> and Hiroshi Kamioka<sup>1</sup>**

<sup>1</sup>Department of Orthodontics, Okayama University Graduate School of Medicine,  
Dentistry and Pharmaceutical Sciences, Okayama, Japan.

<sup>2</sup>Department of Orthodontics, Okayama University Hospital, Okayama, Japan.

<sup>3</sup>Research Fellow of Japan Society for the Promotion of Science, Tokyo, Japan.

<sup>4</sup>Department of Pediatric Hematology/Oncology, Okayama University Hospital,  
Okayama, Japan.

<sup>5</sup>Department of Clinical Application, Center for iPS Cell Research and Application,  
Kyoto University, Kyoto, Japan.

<sup>6</sup>Department of Fundamental Cell Technology, Center for iPS Cell Research and  
Application, Kyoto University, Kyoto, Japan.

*Corresponding author:* Satoru Hayano, D.D.S., Ph.D.

Department of Orthodontics, Okayama University Graduate School of Medicine,  
Dentistry, and Pharmaceutical Sciences

2-5-1 Shikata-cho, Kita-ku, Okayama 700-8525, Japan

Phone: +81-86-235-6691, Fax: +81-86-235-6694, E-mail: shayano@okayama-u.ac.jp

*Corresponding author:* Noriaki Kawanabe, D.D.S., Ph.D.

Department of Orthodontics, Okayama University Graduate School of Medicine,

Dentistry, and Pharmaceutical Sciences

2-5-1 Shikata-cho, Kita-ku, Okayama 700-8525, Japan

Phone: +81-86-235-6692, Fax: +81-86-235-6694, E-mail: kawanabe@md.okayama-

u.ac.jp

**Conflict of Interest:** The authors declare no conflict of interest.

**Keywords:** iPS cell, RPL5, cleft lip and palate, chondrocyte, Diamond-Blackfan

Anemia

Word count: 3517 (including the abstract and excluding references, tables and figures)

Abstract word count: 181

Table/Figure count: 5

Reference count: 41

## Abbreviations

**DBA** Diamond-Blackfan anemia

**RP** Ribosomal protein

**MSC** Mesenchymal stem cell

**MDM2** Murine double minute 2

**iPSC** Induced pluripotent stem cell

**TUNEL** TdT-mediated dUTP nick-end labeling

**SOX9** SRY-box9

46	ACAN	Aggrecan
47	COL10A1	Collagen Type X Alpha 1 Chain
48	OSX	Osterix
49	OPN	Osteopontin
50	BSP	Bone sialoprotein
51	p53	Tumor protein p53
52	BAX	BCL2 Associated X
53	CASP9	Caspase 9
54	RT-qPCR	Quantitative real-time reverse transcription polymerase chain
55	reaction	

## ABSTRACT

Diamond-Blackfan anemia (DBA) is a genetic disorder caused by mutations in genes encoding ribosomal proteins and characterized by erythroid aplasia and various physical abnormalities. Although accumulating evidence suggests that defective ribosome biogenesis leads to p53-mediated apoptosis in erythroid progenitor cells, little is known regarding the underlying causes of the physical abnormalities. In this study, we established induced pluripotent stem cells from a DBA patient with *RPL5* haploinsufficiency. These cells retained the ability to differentiate into osteoblasts and chondrocytes. However, *RPL5* haploinsufficiency impaired the production of mucins and increased apoptosis in differentiated chondrocytes. Increased expression of the pro-apoptotic genes *BAX* and *CASP9* further indicated that *RPL5* haploinsufficiency triggered p53-mediated apoptosis in chondrocytes. MDM2, the primary negative regulator of p53, plays a crucial role in erythroid aplasia in DBA patient. We found the phosphorylation level of MDM2 was significantly decreased in *RPL5* haploinsufficient chondrocytes. In stark contrast, we found no evidence that *RPL5* haploinsufficiency impaired osteogenesis. Collectively, our data support a model in which *RPL5* haploinsufficiency specifically induces p53-mediated apoptosis in chondrocytes through MDM2 inhibition, which leads to physical abnormalities in DBA patients.

## INTRODUCTION

Diamond-Blackfan anemia (DBA) is characterized by erythroid aplasia, and most of the patients carry mutations in structural genes encoding ribosomal proteins (RPs).<sup>1</sup> About 40% of DBA patients also suffer from growth retardation and/or multiple physical abnormalities, particularly in the craniofacial region, upper limbs, heart, and urinary system.<sup>2,3</sup> So far, 78% of all DBA cases have been associated with mutations or deletions in at least 19 different RP-encoding genes.<sup>4</sup> Among these, *RPS19*, which encodes a component of the 40S ribosomal subunit, is the most commonly affected gene and is mutated in 25% of all DBA cases.<sup>5</sup> In contrast, mutations in *RPL5*, which encodes a component of the 60S ribosomal subunit, are found in only 6.6% of all DBA cases. Notably, DBA patients harboring *RPL5* mutations exhibit a higher frequency of physical abnormalities (70%) than those with *RPS19* mutations (46%).<sup>6</sup> Moreover, *RPL5* mutations have been reported to cause phenotypes such as micrognathia and short stature, which suggest defective chondrogenesis.<sup>6</sup>

Recent reports on the pathophysiology of DBA have suggested that ribosomal dysfunction can activate tumor protein p53 (p53)-mediated apoptosis in cells of the erythroid lineage. Indeed, *in vitro* inhibition of RP-encoding genes such as *RPS14* or *RPS19* results in p53 accumulation and triggers apoptosis in human hematopoietic progenitor cells.<sup>7</sup> The murine double minute 2 (MDM2) E3 ubiquitin ligase is the primary negative regulator of p53 and promotes its degradation, keeping p53 at low levels in unstressed cells.<sup>8</sup> However, MDM2-mediated ubiquitylation of p53 is inhibited by various cellular stresses, such as DNA damage or nucleolar stress, which can result in the activation of the p53 signaling pathway.<sup>9</sup>

Remarkably, recent reports have suggested that ribosomal dysfunction could cause nucleolar stress, and several RPs have been reported to inhibit MDM2 activity.<sup>10,11</sup> Under normal conditions, RPs are transported from the cytosol into the nucleolus, where ribosomal RNAs are transcribed, to assemble pre-ribosomal particles.<sup>12</sup> However, mutations in RP-encoding genes can impair ribosome biogenesis, which increases the availability of ribosome-free forms of RPs. Subsequently, some of these ribosome-free RPs can bind to MDM2 and inhibit MDM2-mediated p53 degradation.<sup>13,14</sup> Furthermore, inhibition of *RPS14* or *RPS19* expression has been shown to induce nucleolar stress and activate the p53 signaling pathway in erythroid progenitor cells.<sup>7</sup>

Although dysregulation of MDM2-mediated p53 degradation appears to play a crucial role in the hematopoietic defects in DBA patients, the molecular mechanisms underlying DBA-related physical abnormalities remain elusive. Nevertheless, a previous study has established that in a zebrafish model of DBA, *RPS19* deficiency is associated with severe cartilage defects and impairs ribosomal biogenesis, which activates p53-mediated apoptosis.<sup>15</sup> To the best of our knowledge, there is no published study focusing on the molecular causes underlying DBA-related skeletal abnormalities in human. In this study, we established induced pluripotent stem cells (iPSCs) from peripheral blood cells of an *RPL5* haploinsufficient DBA patient and investigated the molecular mechanisms underlying the physical abnormalities in DBA patients.

## **MATERIALS AND METHODS**

### **Study approval**

The study protocol was approved by the institutional ethics committee of Okayama University (approval number 1608-030) and Kyoto University (approval number R0091/g0259). All methods were performed following the relevant guidelines and regulations. Written informed consent for inclusion in this study and disclosure of clinical information was obtained from all the participants.

#### **Nucleic acid isolation and Sanger sequencing**

After the informed consent process, peripheral blood mononuclear cells were isolated using a BD Vacutainer (BD Biosciences, San Jose, CA, USA) according to the manufacturer's instructions. Genomic DNA was isolated using Wizard genomic DNA purification kit (Promega, Madison, WI, USA). Individual RPL5 exons with flanking regions were PCR-amplified, and corresponding PCR products were isolated from an agarose gel by QIAquick Gel Extraction Kit (Qiagen, Hilden, Germany). The isolated DNA was used for direct sequencing on Applied Biosystems 3130xl Genetic Analyzer (Applied Biosystems, Foster City, CA, USA).

#### **Establishment of iPSCs**

Peripheral blood cells from a 10-year-old male DBA patient (CiRA-j-0084) and a healthy sib (CiRA-j-0086, for control experiments) were used to generate iPSCs as previously described.<sup>16</sup> Briefly, peripheral blood mononuclear cells were cultured for 5 days in StemSpan-ACF medium (STEMCELL Technologies, Vancouver, BC, Canada) supplemented with 100 ng/ml stem cell factor (R&D Systems, Minneapolis, MN, USA), 100 ng/ml thrombopoietin (R&D Systems), 100 ng/ml Flt ligand (R&D Systems), 50

ng/ml IL-6 (R&D Systems), and 20 ng/ml IL-3 (R&D Systems). Next,  $1-2 \times 10^6$  peripheral blood mononuclear cells were transfected with 3  $\mu$ g of episomal plasmids (600 ng of each: pCE-hOCT3/4, pCE-hSK, pCE-hUL, pCE-mp53DD, and pCXB-EBNA1) using the Amaxa Human CD34<sup>+</sup> Cell Nucleofector Kit (Lonza, Basel, Switzerland) and a Nucleofector 2b device (Lonza) according to the manufacturer's instructions. Electroporated cells were seeded into tissue-culture plates coated with iMatrix-511 (Nippi, Tokyo, Japan) and cultured in StemSpan-ACF medium supplemented with the cytokines listed above. The culture medium was gradually replaced with StemFit AK03 medium (Ajinomoto, Tokyo, Japan), and 2–3 weeks after transduction, individual colonies were isolated and expanded.

Established iPSCs were maintained at 37°C in a humidified incubator with an atmosphere containing 5% CO<sub>2</sub> and 21% O<sub>2</sub>, using iMatrix511-coated tissue-culture plates and StemFit AK03 medium. Established iPSCs were passaged by dissociation into single cells with TrypLE Select (Life Technologies, Carlsbad, CA, USA).

#### **Differentiation of iPSCs into mesenchymal stem cells (MSCs)**

MSCs were derived from iPSCs as previously described.<sup>17,18</sup> Briefly, StemFit AK03 medium was replaced with Alpha Minimum Essential Medium ( $\alpha$ -MEM; Invitrogen, Carlsbad, CA, USA) supplemented with 10% stem cell-qualified fetal bovine serum (HyClone, Logan, UT, USA), 100 units/ml penicillin (Invitrogen), 100 mg/ml streptomycin (Invitrogen), 4 mg/ml human basic fibroblast growth factor (R&D Systems), and 10 mM non-essential amino acids (Gibco, Grand Island, NY, USA). The culture medium was replaced every day for 14 days. On day 14, cells were detached

from the iMatrix511-coated Petri dishes using 5 % Trypsin/EDTA (Life Technologies) and transferred into CELLSTAR cell culture dishes (Sigma, St. Louis, MO, USA). Differentiated MSCs were maintained using low glucose Dulbecco's modified Eagle medium (DMEM; Life Technologies) supplemented with 15% stem cell-qualified fetal bovine serum, 100 units/ml penicillin, and 100 mg/ml streptomycin. The culture medium was replaced twice a week.

#### **Osteogenic and chondrogenic differentiation assays**

For osteogenic differentiation, MSCs were cultured in  $\alpha$ -MEM supplemented with 10% stem cell-qualified fetal bovine serum, 100 units/ml penicillin, 100 mg/ml streptomycin, 100 nM dexamethasone (Sigma), 0.05 mM L-ascorbic acid (Sigma), and 10 mM  $\beta$ -glycerophosphate (Sigma). The culture medium was replaced twice a week, and after 3 weeks, Alizarin Red S (Nakarai Tesque, Kyoto, Japan) staining was used to assess osteogenic differentiation.

For chondrogenic differentiation, approximately  $3 \times 10^5$  MSCs aliquots were pelleted in 15 ml polypropylene conical tubes (Sigma) and then cultured by pellet culture method in presence of high-glucose DMEM (Life Technologies) supplemented with 100 units/ml penicillin, 100 mg/ml streptomycin, 100 nM dexamethasone, 1 mM sodium pyruvate (Sigma), 0.17 mM L-ascorbic acid, 0.35 mM L-proline (Sigma), 10% ITS+ Universal Culture Supplement Premix (BD Biosciences), and 10 ng/mL human transforming growth factor beta 3 (R&D Systems). The culture medium was replaced twice a week, and after 3 weeks, Alcian Blue (Sigma) staining was performed to assess chondrogenic differentiation. BX-51 microscope (Olympus, Tokyo, Japan) with a DP-

72 CCD camera (Olympus) was used to obtain the images. The captured images were binarized and positive area for Alcian Blue or Alizarin Red was measured by ImageJ software (NIH, Bethesda, MD, USA).

#### **Immunoblot analysis**

MSCs of each group were lysed in RIPA buffer (Merck, Darmstadt, Germany). The resulting lysates were run on 10% Mini-Protean TGX gels (Bio-Rad, CA, USA) and transferred to Immobilon-P Transfer Membrane (Merck). The following antibodies were used for immunodetection: RPL5 (1:1,000, 14568, Cell Signaling Technology, MA, USA) and  $\beta$ -actin (1:2,000, A5441, Sigma).

#### **TdT-mediated dUTP nick-end labeling (TUNEL) assay and immunofluorescence**

Differentiated chondrocytes and osteoblasts were fixed overnight at 4°C in 4% paraformaldehyde (Nakarai Tesque). Fixed chondrocytes were embedded in paraffin and 6- $\mu$ m-thick sections were cut. The TUNEL *In Situ* Cell Death Detection Kit, fluorescein, (Roche Applied Bioscience, Mannheim, Germany) was used to measure cell death according to the manufacturer's instructions. Fluorescence images were processed using ImageJ software (NIH). For immunostaining, fixed chondrocyte masses were stained with monoclonal anti-MDM2 (1:100, SC-965, Santa Cruz Biotechnology, CA, USA), polyclonal anti-phospho-MDM2 (Serine 166) (1:100, ab131355, Abcam, Cambridge, MA, USA) at 4°C overnight. **The proliferation associated nuclear antigen was detected with anti-Ki67 (1:200, ab15580, Abcam).** Alexa Fluor 594-conjugated goat anti mouse and Alexa Fluor 488-conjugated goat anti rabbit were used as secondary

antibodies. Then, the sections were counterstained with 4',6-diamidino-2-phenylindole (DAPI; 1:1,000, D9542, Sigma) and mounted with fluorescent mounting medium (Dako, Glostrup, Denmark).

## **Quantitative real-time reverse transcription polymerase chain reaction (RT-qPCR)**

Total RNA was isolated using ISOGEN reagent (Nippon Gene, Tokyo, Japan) and reverse-transcribed using the ReverTra Ace qPCR RT Kit (Toyobo, Osaka, Japan), both according to the manufacturer's instructions. The relative levels of cDNA products were analyzed by qPCR analyses using gene-specific primers and the SYBR Green Realtime PCR Master Mix (Toyobo) according to the manufacturer's instructions. The qPCR analyses were performed using a LightCycler 96 System (Roche Life Science, Mannheim, Germany), and the relative expression was calculated and normalized using the  $2^{-\Delta \Delta C_t}$  method with *GAPDH* as the internal reference.

## **Statistical analyses**

All analyses were performed using SPSS version 18 software (IBM, Somers, NY, USA). All data are expressed as mean values  $\pm$  standard deviation (SD) of at least three independent experiments. The difference between two groups was considered statistically significant for Student's *t*-test *p* values  $< 0.05$ .

## **RESULTS**

### **Clinical features of the DBA patient**

To investigate the underlying causes of the physical phenotypes in DBA patients, we

established DBA-specific human iPSCs from peripheral blood cells of a 10-year-old male DBA patient. Our mutation analysis confirmed that the patient carried a heterozygous 2-base deletion in exon 3 of *RPL5* (c.175\_176delGA), which resulted in a frameshift mutation (p.D59Yfs\*53) with premature RPL5 protein termination (Fig. 1a-c). Expression of RPL5 protein level was reduced in MSCs established from iPSCs of the DBA patient (Fig. 1d).

In addition to macrocytic anemia, the *RPL5* haploinsufficient DBA patient presented multiple physical abnormalities, which included short stature, micrognathia, cleft lip and cleft palate, hypertelorism, snub nose, congenital missing permanent teeth, and pulmonary atresia (Fig. 2a-f). However, cephalometric radiographs suggested that the patient presented no apparent abnormalities in intramembranous bones, such as the clavicles and cranial bones (Fig. 2g, h).

### **Chondrogenic and osteogenic differentiation of RPL5 haploinsufficient MSCs**

To gain some insight into the molecular mechanisms underlying physical phenotypes in DBA patients, we derived MSCs from *RPL5* haploinsufficient iPSCs and assessed their ability to differentiate into chondrocytes and osteoblasts. We first used RT-qPCR to measure the expression levels of *SOX9*, *ACAN*, and *COL10A1*, three specific markers of chondrogenic differentiation, and *OSX*, *OPN*, and *BSP*, three osteogenic-specific genes. After 3 weeks of culture in chondrogenic or osteogenic differentiation medium, the expression levels of the three chondrogenic or osteogenic markers were increased in both *RPL5* haploinsufficient and control cells (Fig. 3a, b).

To further assess cell differentiation, we used Alcian Blue and Alizarin Red S

to detect mucins in chondrocytes cultures and calcium deposition in osteoblasts cultures, respectively. Importantly, staining confirmed the presence of differentiated chondrocytes and osteoblasts in both *RPL5* haploinsufficient and control cells (Fig. 3c, d). However, the quantification of the Alcian Blue-positive staining areas showed that *RPL5* haploinsufficient chondrocytes produced less mucins than control chondrocytes (Fig. 3e), whereas Alizarin Red S-positive staining areas were comparable in the *RPL5* haploinsufficient and control osteoblasts (Fig. 3f). We also evaluated *RPL5* production level in cell lysates of differentiated chondrocytes and osteoblasts from both groups. Western blot analysis showed that *RPL5* level was significantly lower in *RPL5* haploinsufficient chondrocytes and osteoblasts than those of control group (Fig. 3g, h). When we focused on the *RPL5* level in the individual groups, no significant tissue-specific differences were found between chondrocyte and osteoblasts (Fig. 3h).

#### **Apoptosis in *RPL5* haploinsufficient chondrocytes and osteoblasts**

Previous studies investigating the underlying causes of anemia in DBA patients have reported an increase in p53-mediated cell death in human erythroid progenitor cells.<sup>7</sup> Therefore, we hypothesized that cell death could be responsible for the reduction of Alcian Blue-positive staining areas in the chondrocytes derived from the *RPL5* haploinsufficient DBA patient. Using the TUNEL assay to assess apoptosis, we found that the number of apoptotic cells was low in control chondrocyte masses but increased significantly in *RPL5* haploinsufficient chondrocyte masses, particularly in the central area of the specimen (Fig. 4a, c).

To examine the potential relationship between the p53 signaling pathway and

apoptosis observed in *RPL5* haploinsufficient chondrocyte masses, cells were harvested at different time points and the expression levels of *P53* and its target genes *BAX* and *CASP9* were measured by RT-qPCR. Although *P53* expression tended to decrease after differentiation in both *RPL5* haploinsufficient and control chondrocytes, the changes observed were not significant (Fig. 4e). Remarkably, while there was no notable activation of the p53 signaling pathway in control chondrocytes, *BAX* and *CASP9* expression increased significantly in *RPL5* haploinsufficient chondrocytes at two and three weeks after culture, despite the lack of increase in *P53* expression (Fig. 4e). Importantly, the number of apoptotic cells after differentiation (Fig. 4b, d) and the expression levels of *P53*, *BAX*, and *CASP9* (Fig. 4f) were not significantly different between *RPL5* haploinsufficient and control osteoblasts at all time points.

To investigate the role of *RPL5* in cell proliferation, we counted the number of Ki67-positive proliferating chondrocytes or osteoblasts (Fig. 4g, h) and quantified the ratio of these cells as a percentage of the total cell number (Fig. 4i, j). The ratio of Ki67-positive proliferating chondrocytes and osteoblasts were comparable between *RPL5* haploinsufficient and control groups (Fig. 4i, j), indicating that the *RPL5* mutation does not alter cell proliferation in the differentiated chondrocytes and osteoblasts.

To dissect the molecular mechanism governing how *RPL5* haploinsufficiency results in cell death in the DBA chondrocytes, we examined the phosphorylation levels of MDM2 by immunostaining (Fig. 4g). The number of phospho-MDM2 positive cells was significantly reduced in DBA chondrocytes (Fig. 4h), that is coincide with the previous report demonstrating mutation of RP gene reduces phosphorylation levels of MDM2 in HCT116 cells.<sup>19</sup>

## MDM2 activity in chondrocytes

Several studies have shown that RPs, including RPL5, RPL11, RPL23, and RPS7, can bind to MDM2 and impair MDM2-mediated p53 degradation in DBA patients.<sup>20,21</sup> To further dissect the molecular mechanisms governing how *RPL5* haploinsufficiency results in cell death in the DBA chondrocytes (Fig. 4a, c) and investigate the potential involvement of MDM2, we examined the phosphorylation levels of MDM2 by immunostaining (Fig. 4g). Remarkably, the number of phospho-MDM2 positive cells was significantly reduced in DBA chondrocytes (Fig. 4h), that is coincide with the previous report demonstrating mutation of RP gene reduces phosphorylation levels of MDM2 in HCT116 cells.<sup>19</sup>

## DISCUSSION

Diseases caused by mutations altering the structure or function of ribosomal components are known as ribosomopathies. Although ribosome biogenesis is a ubiquitous and essential process in all cells, the clinical phenotypes of ribosomopathies are highly variable and often tissue-specific.<sup>20</sup> For instance, the 5q deletion syndrome (OMIM: 153550) is caused by heterozygous mutations in *RPS14* and is associated with symptomatic anemia without physical abnormalities.<sup>20,22</sup> In contrast, cartilage-hair hypoplasia (OMIM: 250250) is caused by homozygous or compound heterozygous mutations in *RMRP*, an essential factor in 5.8S rRNA maturation, and is associated with hypoplastic anemia with skeletal abnormalities, including short limbs and short stature.<sup>23,24</sup> Among ribosomopathies, DBA is characterized by its genetic heterogeneity

that results in variable phenotypes in DBA patients. Mutations in *RPL35A*, *RPL11*, and *RPL5* are associated with genitourinary malformations, thumb abnormalities, and craniofacial skeletal abnormalities, respectively.<sup>25</sup> In this study, we focused on the effects of *RPL5* haploinsufficiency on the skeletal elements.

Skeletal development occurs through endochondral and intramembranous ossification. During normal ossification, osteochondroprogenitor cells differentiate into chondrocytes and osteoblasts, which are essential for endochondral and intramembranous ossification, respectively. Therefore, we focused our investigations on chondrocytes and osteoblasts, aiming to elucidate the underlying causes of skeletal abnormalities in *RPL5* haploinsufficient DBA patients. Both *RPL5* haploinsufficient and control chondrocytes showed increased *SOX9* expression, which is essential for the differentiation of proliferating chondrocytes.<sup>26</sup> Similarly, *ACAN* and *COL10A1* expression, which increases in proliferating and hypertrophic chondrocytes, respectively, was equivalent in *RPL5* haploinsufficient and control cells. Although these results suggested that *RPL5* haploinsufficiency does not alter the transcriptome following chondrogenic differentiation, Alcian Blue staining and TUNEL assays highlighted a significant reduction in mucins production and an increase in apoptosis, respectively, in *RPL5* haploinsufficient chondrocytes cultures.

In stark contrast, we found no evidence that *RPL5* haploinsufficiency impaired osteogenesis. This finding is consistent with the observation that the DBA patient did not present apparent abnormalities in membranous bones formation. In agreement with these observations, our previous study on bone morphogenetic protein signaling in a conditional knock-in mouse model showed that p53-mediated apoptosis

was significantly higher in cartilages than in bone tissues during cranial development of the mutant mice.<sup>27</sup> Furthermore, a previous report showed that *P53* knockdown partially rescues cartilage defects in a zebrafish model of DBA.<sup>28</sup> Although the molecular mechanisms underlying the tissue-specificity of ribosomopathies remain unknown, several studies have suggested that heterogeneity in RPs expression levels might explain these tissue-specific variations.<sup>20</sup> According to these reports, we compared *RPL5* production level between chondrocytes and osteoblasts. In the result, *RPL5* level was comparable, and we could not find such tissue-specific difference explaining why apoptosis was higher in *RPL5* insufficient chondrocyte than osteoblast. To understand the mechanism underlying the tissue-specific variation, further study about nucleolar stress and how the stress is integrated to p53 apoptotic pathway in each tissue is required.

Intriguingly, our RT-qPCR analyses revealed that the p53 apoptotic pathway was activated in *RPL5* haploinsufficient chondrocytes, as shown by the increased expression of the pro-apoptotic factors *BAX* and *CASP9*. However, p53-mediated apoptosis occurred without induction of *P53* expression, which instead slightly decreased in both *RPL5* haploinsufficient and control cells. In agreement with this observation, previous studies have reported that homeostatic expression of *P53* is essential to maintain the stemness and proliferation properties of MSCs.<sup>29,30</sup>

In general, p53 is activated in response to a variety of cellular stresses, which trigger its nuclear accumulation, and is inhibited by ubiquitylation, which induces its degradation.<sup>31,32</sup> MDM2 is recognized as a critical E3 ubiquitin ligase in the p53 regulatory network,<sup>33</sup> and accumulating evidence suggests that various RPs, including

RPL5, RPS7, RPS14, RPL11, RPL23, RPL26, and RPS27, can bind MDM2 and inhibit MDM2-mediated p53 degradation.<sup>21,33-40</sup> In our study, phosphorylation of MDM2 was decreased, and cell death was increased in *RPL5* haploinsufficient chondrocytes indicating that MDM2 played an important regulatory role in the induction of p53-mediated apoptosis and the productions of mucins by chondrocytes. Importantly, it has been previously suggested that activation of the p53 apoptotic pathway without increased *P53* expression could be mediated by post-transcriptional modifications of p53.<sup>7</sup> Collectively, it is plausible to speculate that *RPL5* haploinsufficiency caused decrease of MDM2 phosphorylation, which inhibited its nuclear import and ubiquitin ligase activity, and consequently the p53 apoptotic pathway was activated (Fig. 5).

Nevertheless, p53-independent pathways have also been proposed to play a role in DBA pathogenesis,<sup>41</sup> and at this stage, we cannot exclude the possibility that alterations in these pathways, which might involve MDM2, contributed to the phenotypes associated with *RPL5* haploinsufficiency.

In conclusion, our DBA iPSCs model revealed that *RPL5* haploinsufficiency specifically increased cell death during chondrogenesis, but not osteogenesis, via MDM2 inhibition and activation of the p53 apoptotic pathway in chondrocytes. These findings shed light on the molecular mechanisms underlying the physical abnormalities found in DBA patients. However, further studies will be required to fully understand the tissue-specific role of *RPL5*, as well as the more general mechanisms leading to tissue-specific defects in DBA and other ribosomopathies.

## ACKNOWLEDGEMENT

The authors are very grateful to the patient and his family for their participation in the study.

#### **DISCLOSURE STATEMENT**

None declared.

#### **AUTHOR CONTRIBUTIONS**

YF contributed to data acquisition; SH contributed to design, data acquisition, analysis and interpretation, drafted and critically revised the manuscript; NK contributed to design, data acquisition, and interpretation; ZW contributed to data acquisition; AS contributed to design of the human subject research aspect of this project; MKS and IA contributed to iPS cell generation; HK contributed to data interpretation, critically revised the manuscript. All authors gave final approval and agree to be accountable for all aspects of the work.

#### **REFERENCES**

- 1 Lipton JM, Ellis SR. Diamond-Blackfan anemia: diagnosis, treatment, and molecular pathogenesis. *Hematol Oncol Clin North Am* 2009; **23**: 261-82.
- 2 Ball SE, McGuckin CP, Jenkins G, Gordon-Smith EC. Diamond-Blackfan anaemia in the U.K.: analysis of 80 cases from a 20-year birth cohort. *Br J Haematol* 1996; **94**: 645-53.
- 3 Willig TN, Niemeyer CM, Leblanc T, Tiemann C, Robert A, Budde J, Lambilliotte

367 A, Kohne E, Souillet G, Eber S, et al. Identification of new prognosis factors from  
 368 the clinical and epidemiologic analysis of a registry of 229 Diamond-Blackfan  
 369 anemia patients. DBA group of Société d'Hématologie et d'Immunologie  
 370 Pédiatrique (SHIP), Gesellschaft für Pädiatrische Onkologie und Hämatologie  
 371 (GPOH), and the European Society for Pediatric Hematology and Immunology  
 372 (ESPHI). *Pediatr Res* 1999; **46**: 553-61.

373 4 Jacob CU, Jeffrey MV, Shideh K, Michael HG, Daniel Y, Leif SL, Robert EH,  
 374 Nour JA, Claudia F, Giulio G, et al. The Genetic Landscape of Diamond-Blackfan  
 375 Anemia. *Am J Hum Genet* 2018; **103**: 930-47.

376 5 Gazda HT, Zhong R, Long L, Niewiadomska E, Lipton JM, Ploszynska A, Zaucha  
 377 JM, Vlachos A, Atsidaftos E, Viskochil DH, et al. RNA and protein evidence for  
 378 haplo-insufficiency in Diamond-Blackfan anaemia patients with *RPS19* mutations.  
 379 *Br J Haematol* 2004; **127**: 105-13.

380 6 Gazda HT, Sheen MR, Vlachos A, Choesmel V, O'Donohue MF, Schneider H,  
 381 Darras N, Hasman C, Sieff CA, Newburger P, et al. Ribosomal protein L5 and L11  
 382 mutations are associated with cleft palate and abnormal thumbs in Diamond-  
 383 Blackfan anemia patients. *Am J Hum Genet* 2008; **83**: 769-80.

384 7 Dutt S, Narla A, Lin K, Mullally A, Abayasekara N, Megerdichian C, Wilson FH,  
 385 Currie T, Khanna-Gupta A, Berliner N et al. Haploinsufficiency for ribosomal  
 386 protein genes causes selective activation of p53 in human erythroid progenitor cells.  
 387 *Blood* 2011; **117**: 2567-76.

- 388 8 Hock AK, Vousden KH. The role of ubiquitin modification in the regulation of p53.  
389 *Biochim Biophys Acta* 2014; **1843**:137-49.
- 390 9 Shieh SY, Ikeda M, Taya Y, Prives C. DNA damage-induced phosphorylation of  
391 p53 alleviates inhibition by MDM2. *Cell* 1997; **91**: 325-34.
- 392 10 Sun XX, Dai MS, Lu H. 5-fluorouracil activation of p53 involves an MDM2-  
393 ribosomal protein interaction. *J Biol Chem* 2007; **282**: 8052-59.
- 394 11 Lessard F, Brakier-Gingras L, Ferbeyre G. Ribosomal Proteins Control Tumor  
395 Suppressor Pathways in Response to Nucleolar Stress. *Bioessays* 2019; **41**:  
396 e1800183.
- 397 12 Peña C, Hurt E, Panse VG. Eukaryotic ribosome assembly, transport and quality  
398 control. *Nat Struct Mol Biol* 2017; **24**: 689-99.
- 399 13 Donati G, Peddigari S, Mercer CA, Thomas G. 5S ribosomal RNA is an essential  
400 component of a nascent ribosomal precursor complex that regulates the Hdm2-p53  
401 checkpoint. *Cell Rep* 2013; **4**: 87-98.
- 402 14 Sloan KE, Bohnsack MT, Watkins NJ. The 5S RNP couples p53 homeostasis to  
403 ribosome biogenesis and nucleolar stress. *Cell Rep* 2013; **5**: 237-47.
- 404 15 Danilova N, Sakamoto KM, Lin S. Ribosomal protein S19 deficiency in zebrafish  
405 leads to developmental abnormalities and defective erythropoiesis through  
406 activation of p53 protein family. *Blood* 2008; **112**: 5228-37.
- 407 16 Okita K, Yamakawa T, Matsumura Y, Sato Y, Amano N, Watanabe A, Goshima N,  
408 Yamanaka S. An efficient nonviral method to generate integration-free human-

409 induced pluripotent stem cells from cord blood and peripheral blood cells. *Stem*  
410 *Cells* 2013; **31**: 458-66.

411 17 Nejadnik H, Diecke S, Lenkov OD, Chapelin F, Donig J, Tong X, Derugin N, Chan  
412 RC, Gaur A, Yang F, et al. Improved approach for chondrogenic differentiation of  
413 human induced pluripotent stem cells. *Stem Cell Rev* 2015; **11**: 242-53.

414 18 Kimbrel EA, Kouris NA, Yavanian GJ, Chu J, Qin Y, Chan A, Singh RP, McCurdy  
415 D, Gordon L, Levinson RD, et al. Mesenchymal stem cell population derived from  
416 human pluripotent stem cells displays potent immunomodulatory and therapeutic  
417 properties. *Stem Cells Dev* 2014; **23**: 1611-24.

418 19 Sagar V, Caldarola S, Aria V, Monteleone V, Fuoco C, Gargioli C, Cannata S,  
419 Loreni F. PIM1 destabilization activates a p53-dependent response to ribosomal  
420 stress in cancer cells. *Oncotarget* 2016; **7**: 23837-49.

421 20 Nakhoul H, Ke J, Zhou X, Liao W, Zeng SX, Lu H. Ribosomopathies: mechanisms  
422 of disease. *Clin Med Insights Blood Disord* 2014; **14**: 7-16.

423 21 Chen D, Zhang Z, Li M, Wang W, Li Y, Rayburn ER, Hill DL, Wang H, Zhang R.  
424 Ribosomal protein S7 as a novel modulator of p53-MDM2 interaction: binding to  
425 MDM2, stabilization of p53 protein, and activation of p53 function. *Oncogene*  
426 2007; **26**: 5029-37.

427 22 Tinegate H, Gaunt L, Hamilton PJ. The 5q- syndrome: an underdiagnosed form of  
428 macrocytic anaemia. *Br J Haematol* 1983; **54**: 103-10.

429 23 Mäkitie O, Sulisalo T, de la Chapelle A, Kaitila I. Cartilage-hair hypoplasia. *J Med*

430        *Genet* 1995; **32**: 39–43.

431    24   Trainor PA, Merrill AE. Ribosome biogenesis in skeletal development and the  
432        pathogenesis of skeletal disorders. *Biochim Biophys Acta* 2014; **1842**: 769-78.

433    25   Boria I, Garelli E, Gazda HT, Aspesi A, Quarello P, Pavesi E, Ferrante D, Meerpohl  
434        JJ, Kartal M, Da Costa L, et al. The ribosomal basis of Diamond-Blackfan Anemia:  
435        mutation and database update. *Hum Mutat* 2010; **31**: 1269-79.

436    26   Bi W, Huang W, Whitworth DJ, Deng JM, Zhang Z, Behringer RR, de  
437        Crombrughe B. Haploinsufficiency of *Sox9* results in defective cartilage primordia  
438        and premature skeletal mineralization. *Proc Natl Acad Sci U S A* 2001; **98**: 6698-  
439        703.

440    27   Hayano S, Komatsu Y, Pan H, Mishina Y. Augmented BMP signaling in the neural  
441        crest inhibits nasal cartilage morphogenesis by inducing p53-mediated apoptosis.  
442        *Development* 2015; **142**: 1357-67.

443    28   Jia Q, Zhang Q, Zhang Z, Wang Y, Zhang W, Zhou Y, Wan Y, Cheng T, Zhu X,  
444        Fang X, et al. Transcriptome analysis of the zebrafish model of Diamond-Blackfan  
445        anemia from RPS19 deficiency via p53-dependent and -independent pathways.  
446        *PLoS One* 2013; **8**: e71782.

447    29   Boregowda SV, Krishnappa V, Strivelli J, Haga CL, Booker CN, Phinney DG.  
448        Basal p53 expression is indispensable for mesenchymal stem cell integrity. *Cell*  
449        *Death Differ* 2018; **25**: 679-92.

450    30   Armesilla-Diaz A, Elvira G, Silva A. p53 regulates the proliferation, differentiation

451 and spontaneous transformation of mesenchymal stem cells. *Exp Cell Res* 2009;  
 452 **315**: 3598-610.

453 31 Giaccia AJ, Kastan MB. The complexity of p53 modulation: emerging patterns  
 454 from divergent signals. *Genes Dev* 1998; **12**: 2973-83.

455 32 Momand J, Zambetti GP, Olson DC, George D, Levine AJ. The *mdm-2* oncogene  
 456 product forms a complex with the p53 protein and inhibits p53-mediated  
 457 transactivation. *Cell* 1992; **69**: 1237-45.

458 33 Montes de Oca Luna R, Wagner DS, Lozano G. Rescue of early embryonic lethality  
 459 in *mdm2*-deficient mice by deletion of p53. *Nature* 1995; **378**: 203-6.

460 34 Zheng J, Lang Y, Zhang Q, Cui D, Sun H, Jiang L, Chen Z, Zhang R, Gao Y, Tian  
 461 W, et al. Structure of human MDM2 complexed with RPL11 reveals the molecular  
 462 basis of p53 activation. *Genes Dev* 2015; **29**: 1524-34.

463 35 Lohrum MA, Ludwig RL, Kubbutat MH, Hanlon M, Vousden KH. Regulation of  
 464 HDM2 activity by the ribosomal protein L11. *Cancer Cell* 2003; **3**: 577-87.

465 36 Dai MS, Lu H. Inhibition of MDM2-mediated p53 ubiquitination and degradation  
 466 by ribosomal protein L5. *J Biol Chem* 2004; **279**: 44475-82.

467 37 Jin A, Itahana K, O'Keefe K, Zhang Y. Inhibition of HDM2 and activation of p53  
 468 by ribosomal protein L23. *Mol Cell Biol* 2004; **24**: 7669-80.

469 38 Zhang Y, Lu H. Signaling to p53: ribosomal proteins find their way. *Cancer Cell*  
 470 2009; **16**: 369-77.

471 39 Zhou X, Hao Q, Liao J, Zhang Q, Lu H. Ribosomal protein S14 unties the MDM2-

472 p53 loop upon ribosomal stress. *Oncogene* 2013; **32**: 388-96.

473 40 Xiong X, Zhao Y, He H, Sun Y. Ribosomal protein S27-like and S27 interplay with  
474 p53-MDM2 axis as a target, a substrate and a regulator. *Oncogene* 2011; **30**: 1798-  
475 811.

476 41 Aspesi A, Pavesi E, Robotti E, Crescitelli R, Boria I, Avondo F, Moniz H, Da Costa  
477 L, Mohandas N, Roncaglia P, et al. Dissecting the transcriptional phenotype of  
478 ribosomal protein deficiency: implications for Diamond-Blackfan Anemia. *Gene*  
479 2014; **545**: 282-9.

480

481

## Titles and legends to figures

**Figure 1** The DBA patient carries a heterozygous mutation in exon 3 of the *RPL5* gene.

(a) Diagram depicting the changes in *RPL5* mRNA. (b) Mutation analysis by Sanger sequencing. (c) Alignment showing the cDNA and corresponding amino acid sequences of exon 3 of the mutant variant of *RPL5*. (d) Expression level of RPL5 protein in MSCs by immunoblot analysis.

**Figure 2** Images highlighting the clinical features of the 10-year-old DBA patient.

Whole-body (a), intraoral (b, c), and facial photographs (d-f). Frontal (f) and lateral (h) cephalometric radiographs showing clavicles with normal shape (white arrowheads).

**Figure 3** Effects of *RPL5* haploinsufficiency on chondrogenesis and osteogenesis. (a, b)

Total RNA was isolated from MSCs, and differentiated chondrocytes (a) or osteoblasts (b), and mRNA expression levels were measured by RT-qPCR using *GAPDH* as an

internal reference. Histograms showing the relative expression levels of three

chondrogenic differentiation markers, *SOX9*, *ACAN*, and *COL10A1* (a), and three

osteogenic differentiation markers, *OSX*, *OPN*, and *BSP* (b). (c, d) Chondrocytes (c) and

osteoblasts (d) derived from the *RPL5* haploinsufficient DBA patient (DBA) and a

healthy sib (control) were stained with Alcian Blue (c) and Alizarin Red S (d),

respectively. Scale bars are 100  $\mu$ m. (e, f) Quantification of Alcian Blue-positive (e) and

Alizarin Red S-positive (f) staining areas. (g, h) Expression level of RPL5 protein in

chondrocytes and osteoblasts of control and *RPL5* haploinsufficient groups. All data are

mean values  $\pm$  SD ( $n=3$ ), and asterisks indicate the  $p$  values for Student's  $t$ -test

(\* $p < 0.05$  and \*\*  $p < 0.01$ ).

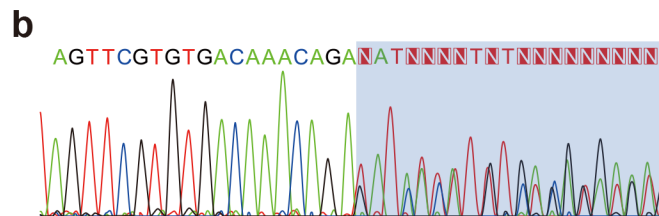
**Figure 4** Effects of *RPL5* haploinsufficiency on p53-mediated apoptosis in chondrocytes and osteoblasts. (a, b) Detection of apoptosis by TUNEL assay in control and *RPL5* haploinsufficient chondrocytes (a) and osteoblasts (b). TUNEL-positive nuclei are labeled with fluorescein (green), and all nuclei are counterstained with DAPI (blue). (c, d) Quantification of apoptosis in control and *RPL5* haploinsufficient chondrocytes (c) and osteoblasts (d). (e, f) Total RNA was isolated from chondrocytes (e) and osteoblasts (f), and mRNA expression levels were measured by RT-qPCR using *GAPDH* as an internal reference. **Line graphs** showing the relative expression levels of three genes involved in the p53 signaling pathway, *P53*, *BAX*, and *CASP9*, in chondrocytes (e) and osteoblasts (f). **(g, h) Detection of proliferating chondrocytes (g) and osteoblasts (h). Immunofluorescent staining of Ki67 is shown in green, and all nuclei are counterstained with DAPI (blue). (i, j) Quantification of cell proliferation in control and *RPL5* haploinsufficient chondrocytes (i) and osteoblasts (j). (k, l) Detection of phospho-MDM2 (Ser166) by immunofluorescence in control and *RPL5* haploinsufficient chondrocytes. Phospho-MDM2 (Ser166) labeled with fluorescein (green), MDM2 are labeled with fluorescein (red), and all nuclei are counterstained with DAPI (blue) (k). Quantification of phospho-MDM2 (Ser166) in control and *RPL5* haploinsufficient chondrocytes (l). All scale bars are 100  $\mu\text{m}$ . All data are mean values  $\pm$  SD ( $n=3$ ), and asterisks indicate the  $p$  values for Student's  $t$ -test (\* $p < 0.05$  and \*\*  $p < 0.01$ ).**

528 **Figure 5** Diagram depicting a model for the decrease of MDM2 phosphorylation and  
529 the activation of p53-mediated apoptosis in *RPL5* haploinsufficient chondrocytes.  
530

**a** *RPL5* c.175\_176delGA (p.D59Yfs\*53)

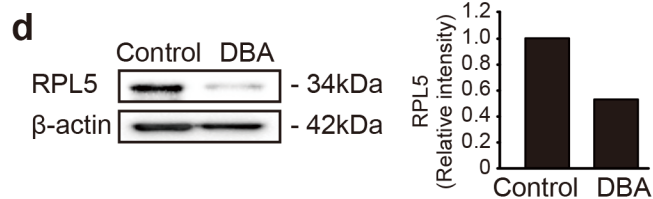
Two base deletion

145 TACAGGATGATAGTTCTGTGTGACAAACAGAGATATCATT  
49 -Y- -R- -M- -I- -V- -R- -V- -T- -N- -R- -D- -I- -I-

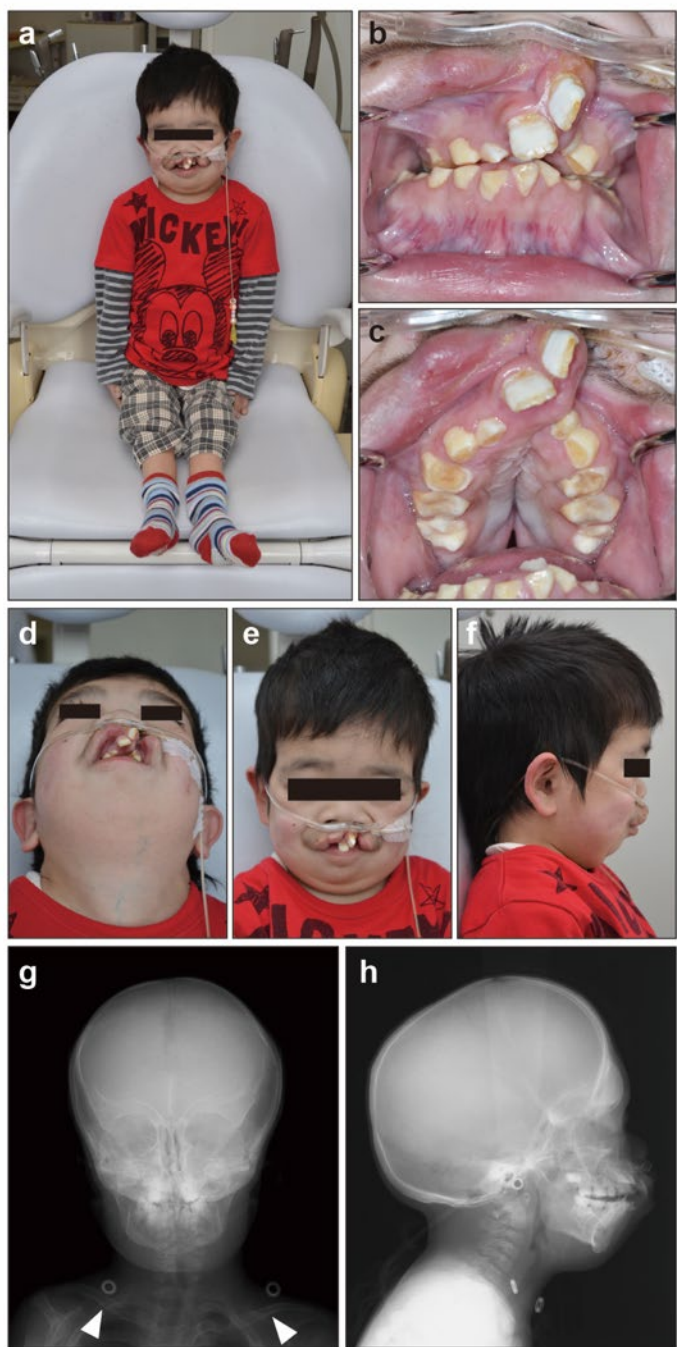


**c**

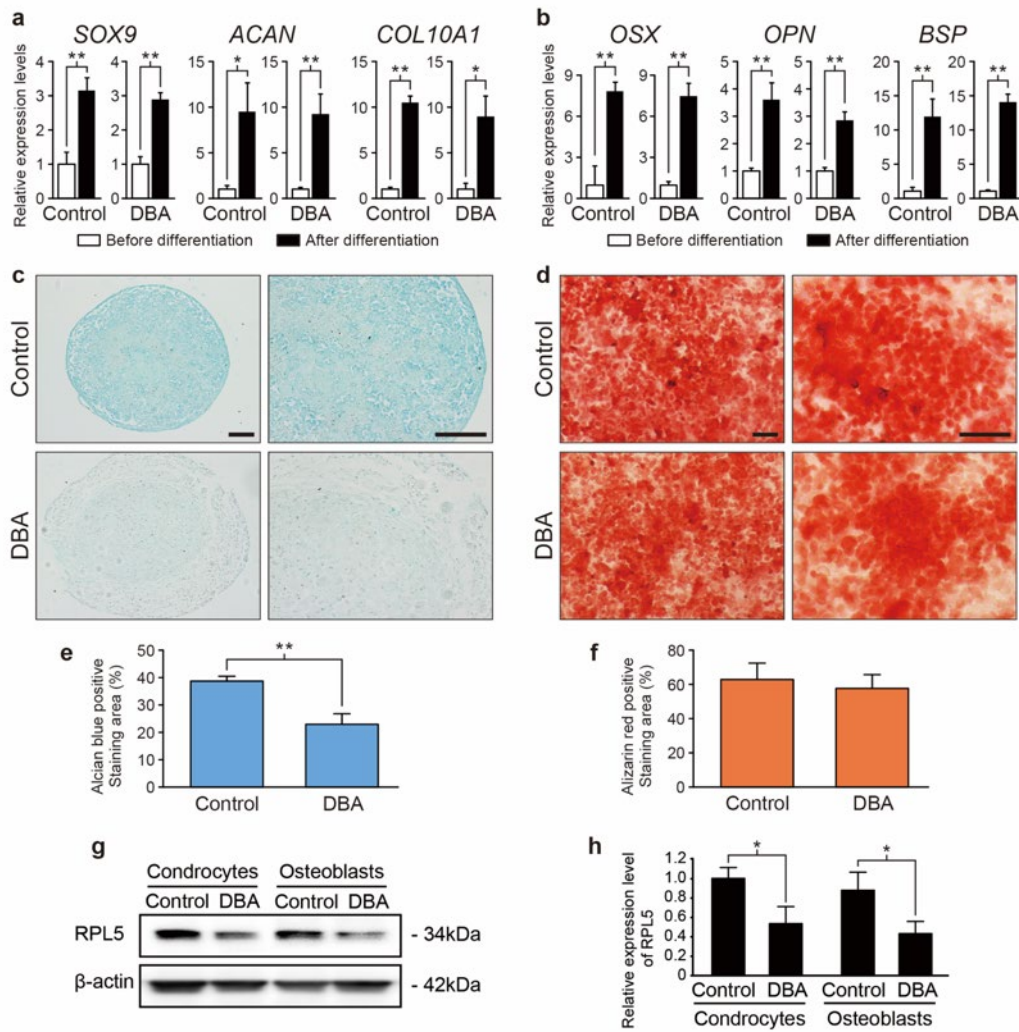
ATGGGGTTTGTAAAGTTGTTAAGAATAAGGCCTACTTT  
-M--G--F--V--K--V--V--K--N--K--A--Y--F--  
AAGAGATACCAAGTGAAATTTAGAAGACGACGAGAGGGT  
-K--R--Y--Q--V--K--F--R--R--R--R--E--G--  
AAAAGTATTATTATGCTCGGAAACGCTTGGTGATACAA  
-K--T--D--Y--Y--A--R--K--R--L--V--I--Q--  
GATAAAAATAAATACAACACACCCAAATACAGGATGATA  
-D--K--N--K--Y--N--T--P--K--Y--R--M--I--  
GTTCGTGTGACAAACAGATATCATTGTGCTGAGATTGCTTA  
-V--R--V--T--N--R--Y--H--L--S--D--C--L--  
TGCCCGTATAGAGGGGATATGATAGTCTGCGCAGCGTA  
-C--P--Y--R--G--G--Y--D--S--L--R--S--V--  
TGCACACGAAGTCCAAAATATGGTGTGAAGGTTGGCCT  
-C--T--R--T--A--K--I--W--C--E--G--W--P--  
GACAAATTATGCTGCAGCATATTGTACTGGCCTGCTGCT  
-D--K--L--C--C--S--I--L--Y--W--P--A--A--  
GGCCCGCAGGCTTCTCAATAGGTTTGGCATGGACAAGAT  
-G--P--Q--A--S--Q--\*-



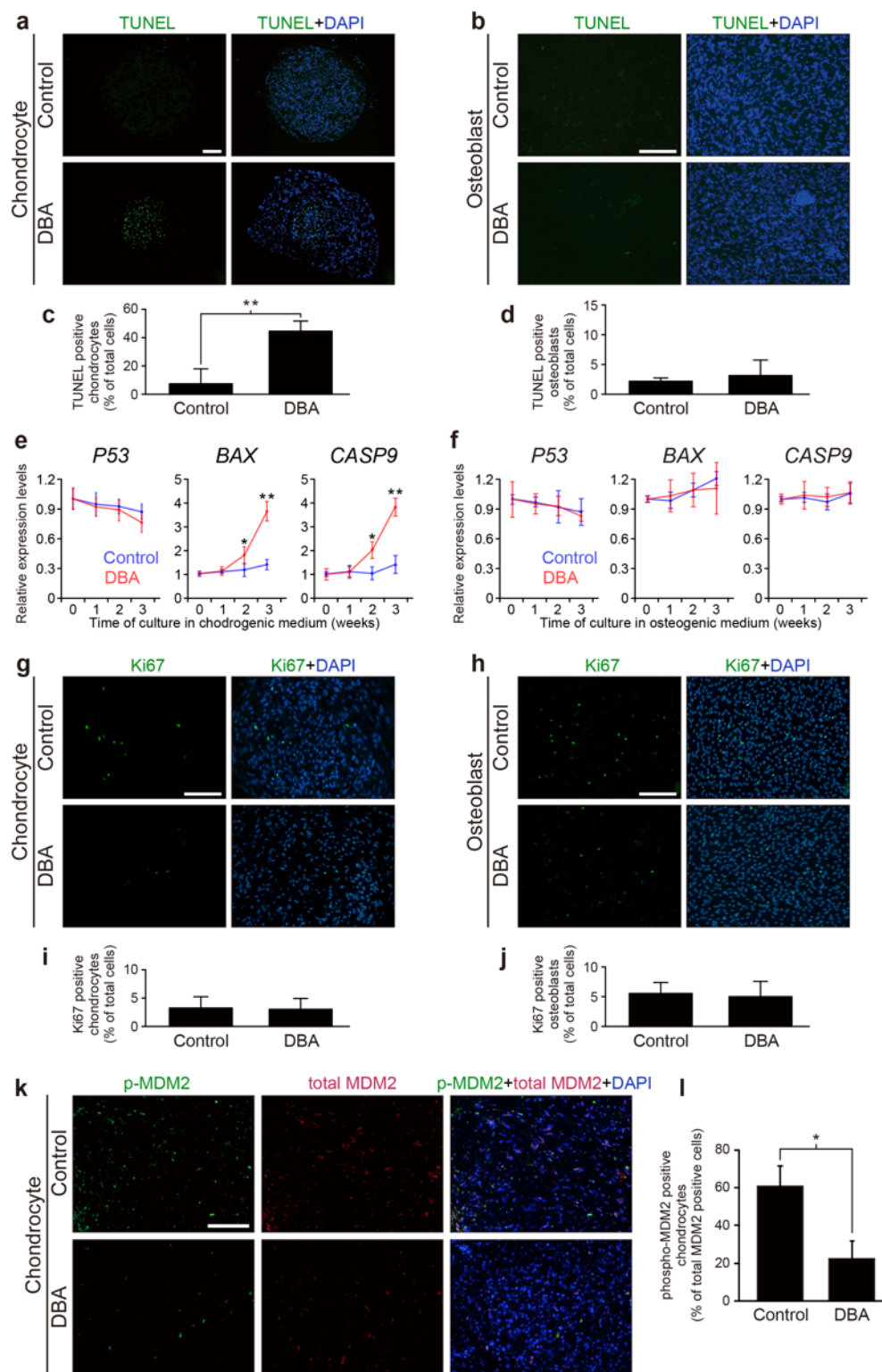
Fukui et al., Fig. 1



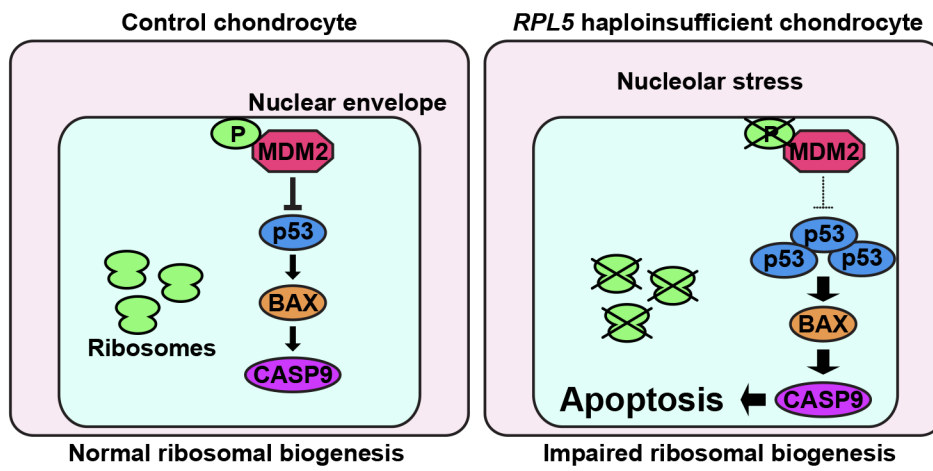
Fukui et al., Fig. 2



Fukui et al., Fig. 3



Fukui et al., Fig. 4



Fukui et al., Fig. 5